CHARACTERIZATION OF THE PRAESEPE STAR CLUSTER BY PHOTOMETRY AND PROPER MOTIONS WITH 2MASS, PPMXL, AND Pan-STARRS

P. F. Wang[1], W. P. Chen[1,2], C. C. Lin[2], A. K. Pandey[3], C. K. Huang[2], N. Panwar[2], C. H. Lee[2], M. F. Tsai[4], C.-H. Tang[4], B. Goldman[5], W. S. Burgett[6], K. C. Chambers[6], P. W. Draper[7], H. Flewelling[6], T. Grav[8], J. N. Heasley[6], K. W. Hodapp[6], M. E. Huber[6], R. Jedicke[6], N. Kaiser[6], R.-P. Kudritzki[6], G. A. Luppino[6], R. H. Lupton[9], E. A. Magnier[6], N. Metcalfe[7], D. G. Monet[10], J. S. Morgan[6], P. M. Onaka[6], P. A. Price[6], C. W. Stubbs[11], W. Sweeney[6], J. L. Tonry[6], R. J. Wainscoat[6], and C. Waters[6]

[1] Department of Physics, National Central University, 300 Jhongda Road, Jhongli 32001, Taiwan
[2] Graduate Institute of Astronomy, National Central University, 300 Jhongda Road, Jhongli 32001, Taiwan
[3] Aryabhatta Research Institute of Observational Sciences, Manora Peak, Nainital 263129, India
[4] Department of Computer Science and Information Engineering, National Central University, 300 Jhongda Road, Jhongli 32001, Taiwan
[5] Max-Planck-Institut für Astronomie, Königstuhl 17, D-69117 Heidelberg, Germany
[6] Institute for Astronomy, University of Hawai'i, 2680 Woodlawn Drive, Honolulu, HI 96822, USA
[7] Department of Physics, Durham University, South Road, Durham DH1 3LE, UK
[8] Department of Physics and Astronomy, Johns Hopkins University, 3400 North Charles Street, Baltimore, MD 21218, USA
[9] Department of Astrophysical Sciences, Princeton University, Princeton, NJ 08544, USA
[10] US Naval Observatory, Flagstaff Station, Flagstaff, AZ 86001, USA
[11] Department of Physics, Harvard University, Cambridge, MA 02138, USA

ABSTRACT

Membership identification is the first step in determining the properties of a star cluster. Low-mass members in particular could be used to trace the dynamical history, such as mass segregation, stellar evaporation, or tidal stripping, of a star cluster in its Galactic environment. We identified member candidates of the intermediate-age Praesepe cluster (M44) with stellar masses ~ 0.11–$2.4\,M_\odot$, using Panoramic Survey Telescope And Rapid Response System and Two Micron All Sky Survey photometry, and PPMXL proper motions. Within a sky area of $3°$ radius, 1040 candidates are identified, of which 96 are new inclusions. Using the same set of selection criteria on field stars, an estimated false positive rate of 16% was determined, suggesting that 872 of the candidates are true members. This most complete and reliable membership list allows us to favor the BT-Settl model over other stellar models. The cluster shows a distinct binary track above the main sequence, with a binary frequency of 20%–40%, and a high occurrence rate of similar mass pairs. The mass function is consistent with that of the disk population but shows a deficit of members below 0.3 solar masses. A clear mass segregation is evidenced, with the lowest-mass members in our sample being evaporated from this disintegrating cluster.

Key words: open clusters and associations: individual (Praesepe) – stars: kinematics and dynamics – stars: luminosity function, mass function

Online-only material: color figures, machine-readable table

1. INTRODUCTION

A star cluster manifests itself as a density concentration of comoving stars in space. Born out of the same molecular cloud, the member stars have similar chemical compositions, are roughly the same age, and at essentially the same distance from us. Therefore, star clusters serve as good test beds to study stellar formation and evolution. In order to diagnose the properties of a star cluster, such as its age, distance, size, spatial distribution, mass function, etc., it is necessary to identify the member stars as completely as possible. In particular, with a sample of members including the lowest mass stars, or even substellar objects, one could trace the dynamical history of an open cluster, e.g., the effect of mass segregation, stellar evaporation, and tidal stripping in the Galactic environment.

Nearby open clusters are useful in the study of their low-mass populations. Praesepe (M44; NGC 2632; the Beehive Cluster) is an example of such a rich (~ 1000 members) and intermediate-age (757 Myr; Gáspár et al. 2009) stellar aggregation in Cancer, as a member of the Hyades moving group (Eggen 1960), also called the Hyades supercluster. Compared to Praesepe, the Hyades cluster itself has a scattered main sequence in the color–magnitude diagram (CMD) due to the significant depth

with respect to its distance. Recently, Goldman et al. (2012) presented a study of the low-mass member in Hyades. The advantages of studying stars in Praesepe are numerous. First, with a distance determination ranging from 170 pc (Reglero & Fabregat 1991) to 184 pc (An et al. 2007), the cluster is close enough to detect low-mass stars or even brown dwarfs. In this work, we adopted a distance measuring 179 ± 2 pc (Gáspár et al. 2009), and a metallicity of [Fe/H] = 0.16 (Carrera & Pancino 2011). Second, the proper motion (PM) of the cluster is distinct from that of the field stars, so contamination is minimized when identifying member stars. Third, in contrast to a star cluster at birth, for which the spatial distribution of members is governed by the parental cloud structure, the stellar distribution in an evolved cluster depends mainly on the interaction between members, from which we could investigate the dynamical evolution of the cluster.

Early PM measurements of Praesepe included the pioneering work of Klein Wassink (1927) to identify bright members within a $1°$ radius of the cluster center, and of Jones & Cudworth (1983) who extended the detection limit to $V \sim 17$ mag to include intermediate-mass members. Wang et al. (1995) combined early data and presented a list of nearly 200 PM members. Using PMs and photometry, Jones & Stauffer (1991) identified a

list of member candidates from $V \sim 9$ to 18 mag within $2°$ of the cluster center. Using optical and infrared photometry, Williams et al. (1995) selected member candidates with mass $M > 0.08 M_\odot$ and obtained a mass function similar to the field, with no evidence of stellar evaporation. Wang et al. (2011) summarized the photometric surveys of Praesepe members down to the hydrogen-burning limit. Notably, Hambly et al. (1995a), with a limiting magnitude of $R \gtrsim 20$ mag, thereby reaching the stellar mass of $\sim 0.1 M_\odot$, derived a rising mass function toward the low-mass end, and presented evidence of mass segregation (Hambly et al. 1995b). With the Two Micron All Sky Survey (2MASS) and the Sloan Digital Sky Survey (SDSS) data, covering a sky area of 100 deg², Adams et al. (2002) extended the lower main sequence to 0.1 $M_\odot$, and determined the radial density profile of member stars. Kraus & Hillenbrand (2007) surveyed a sky area of 300 deg² to identify members, using optical and infrared spectral energy distribution, PM measurements taken from UCAC2 for bright stars, or calculated from USNO-B1, and SDSS positions, reaching almost into the brown-dwarf regime. Their sample of early-type stars is incomplete because of the bright limit of UCAC2, whereas for later-type members incompleteness is caused by the detection limits of USNO-B1 and 2MASS. Recently, Khalaj & Baumgardt (2013) used SDSS and PPMXL data to characterize the stellar members, including the mass segregation effect and binarity.

There have been efforts to identify brown dwarfs in Praesepe. Pinfield et al. (1997) covered 1 deg² down to $I \sim 21$ mag and identified 19 brown-dwarf candidates without spectral confirmation. Chappelle et al. (2005) presented deep optical and near-infrared observations covering 2.6 deg² to a mass limit of 0.06 $M_\odot$. González-García et al. (2006) explored the central 0°.6 radius region, reaching a limit of $i_{SDSS} \sim 24.5$ mag, corresponding to $\sim 0.05–0.13 M_\odot$, and identified one substellar candidate. Boudreault et al. (2010) performed an optical I_c band and near-infrared J and K_s band photometric survey covering 3.1 deg² with detection limits of $I_c \sim 23.4$ mag and $J \sim 20.0$ mag, and found a handful of substellar candidates. The substellar census was augmented by Wang et al. (2011) who, using very deep optical (riz and Y-band) photometry of the central 0.59 deg² region of the cluster, identified a few dozen substellar member candidates. The first spectroscopically confirmed L dwarf member in Praesepe was secured by Boudreault & Lodieu (2013).

The stellar mass function of Praesepe was found to rise until 0.1 $M_\odot$ (Hambly et al. 1995b; Chappelle et al. 2005; Baker et al. 2010; Boudreault et al. 2010), in contrast to the Hyades, which is about the same age but deficient of very low-mass stars and brown dwarfs. Explanations include the possibility that the two clusters have different initial mass functions, or that Praesepe somehow did not experience as much dynamical perturbation in its environments (Bouvier et al. 2008). A recent study, using the UKIRT Infrared Deep Sky Survey (UKIDSS) Galactic Clusters Survey, derived a declining mass function toward lower masses (Boudreault et al. 2012). One of the aims of this work is to secure a sample of highly probable members to address this issue.

The spatial distribution of stars in a cluster is initially governed by the structure in the parental molecular cloud. As a star cluster ages, gravitational scattering by stellar encounters results in mass segregation (Spitzer & Shull 1975), that is, massive stars tend to concentrate toward the center of the cluster, whereas lower mass stars, with a greater velocity dispersion, are distributed out to larger radii. For Praesepe, Hambly et al. (1995a) combined their observations, complete to

$R \sim 20.0$ mag and $I \sim 18.2$ mag, with those of Mermilliod et al. (1990) with $I \lesssim 12$ mag, to show a clear mass segregation effect. While brown dwarfs may have a preferred spatial distribution within a young star cluster (Caballero 2008), they tend to be distributed uniformly as the cluster evolves de la Fuente Marcos & de la Fuente Marcos (2000).

Observational attempts to find and characterize members in a star cluster are often sufficient in depth, but limited in sky coverage, or they cover wide areas but are restricted to only brighter (more massive) members. Studies with large sky coverages usually secure membership on the basis of photometry, lacking PM measurements for faint members. In this paper, we present photometric (2MASS and Panoramic Survey Telescope And Rapid Response System (Pan-STARRS)) and astrometric (PPMXL) diagnostics to select the member candidates in Praesepe. Our sample allows us to characterize the cluster, including the binarity, the mass function, the segregation effect, and its size. We describe the photometric and PM data in Section 2, and how we identified probable members in Section 3. In Section 4, we compare our results with those of the literature, discuss the binarity and present evidence of mass segregation and tidal stripping. A short summary is provided in Section 5.

2. DATA SOURCES

Data used in this study include photometry and PM measurements within a $5°$ radius around the Praesepe center (R.A. = 08^h40^m, decl. = $+19°42'$, J2000). Archival data were taken from the 2MASS Point Sources Catalog, PPMXL, and Pan-STARRS. The 2MASS Point Source Catalog (Skrutskie et al. 2006) has 10σ detection limits of $J \sim 15.8$ mag, $H \sim 15.1$ mag, and $K_s \sim 14.3$ mag, and saturates around 4–5 mag. The typical astrometric accuracy for the brightest unsaturated sources is about 70–80 mas. PPMXL is an all-sky merged catalog based on the USNO-B1 and 2MASS positions of 900 million stars and galaxies, reaching a limiting $V \sim 20$ mag (Roeser et al. 2010). The typical error is less than 2 milliarcseconds (mas) per year for the brightest stars with Tycho-2 (Høg et al. 2000) observations, and is more than 10 mas yr^{-1} at the faint limit.

Pan-STARRS is a wide-field (7 deg²) imaging system, with a 1.8 m, $f/4.4$ telescope (Hodapp et al. 2004), equipped with a 1.4 giga-pixel camera (Tonry et al. 2008). The prototype (PS1), located atop Haleakala, Maui, USA (Kaiser et al. 2010), has been patrolling the entire sky north of $-30°$ declination since mid-2010. Repeat observations of the same patch of sky with a combination of g_{P1}, r_{P1}, i_{P1}, z_{P1}, and y_{P1} bands several times a month produce a large inventory of celestial objects that vary in brightness or in position. Deep static sky images and a catalog of stars and galaxies are also obtained. The PS1 filters differ slightly from those of the SDSS (Abazajian et al. 2009). The g_{P1} filter extends 20 nm redward of g_{SDSS} for greater sensitivity and lower systematics for photometric redshift estimates. SDSS has no corresponding y filter (Tonry et al. 2012b). The limiting magnitudes are $g_{P1} \sim 22.5$ mag, $r_{P1} \sim 22$ mag, $i_{P1} \sim 21.5$ mag, $z_{P1} \sim 21$ mag, and $y_{P1} \sim 19.5$ mag, with the saturation limit of ~ 14 mag. Upon the completion of its 3.5 yr mission by early 2014, PS1 will provide reliable photometry and astrometry. While incremental photometry of PS1 is available at the moment, no PS1 PM data were used in this work because the astrometry still needs to calibrate over the entire sky. The photometric analysis and calibration is described in Magnier et al. (2013). PS1 photometry for each detected object has
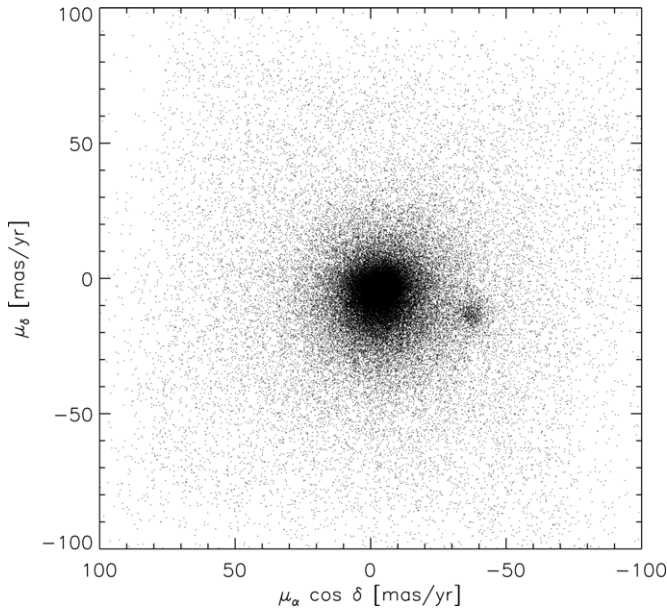
Figure 1. PPMXL proper motion vector point diagram of stars toward Praesepe. Stars within an angular distance of 5° of the cluster center are analyzed. Only stars spatially within the central 2° are displayed here for clarity.

measurements at multiple epochs, but for the work reported here only the average magnitude is used. Therefore, in our study, we made use of the 2MASS photometry for stars too bright for PS1, plus the PS1 photometry for faint stars, and the PPMXL PMs to select and characterize stellar member candidates. While matching counterparts in different star catalogues, 1 arcsecond was used as the coincidence radius among PPMXL, PS1, and 2MASS sources.

3. CANDIDATE SELECTION

Our membership diagnosis relies on grouping in sky position, in PMs, and along the isochrones that are appropriate for the cluster in the infrared and optical CMDs. The sources with 2MASS photometric uncertainties greater than 0.05 mag, roughly reaching $J \sim 15.2$ mag, $H \sim 14.6$ mag, and $K_s \sim 14.5$ mag, were removed from the sample. Candidacy was then further winnowed in the J versus $J - K_s$ CMD by including only objects with $J - K_s$ colors within 0.3 mag from the Padova isochrones (Marigo et al. 2008). This initial, wide range of colors did not allow us to adopt an a priori stellar evolutionary model, but it enabled us to test different models, as demonstrated below.

With the initial photometric sample, we then identified stars with PMs close to that of the cluster. Obviously the choice of the range is a compromise between the quality and the quantity of the candidate list. The optimal range was decided by how the cluster grouping was blended with the field. The PPMXL data toward Praesepe are shown in Figure 1. The PM distribution has two peaks, one for the cluster ($\mu_\alpha \cos \delta \approx -36.5$ mas yr^{-1}, $\mu_\delta \approx -13.5$ mas yr^{-1}) and the other for field stars ($\mu_\alpha \cos \delta \approx -4$ mas yr^{-1}, $\mu_\delta \approx -3$ mas yr^{-1}). The latter is the reflex Galactic motion of the Sun toward this particular line of sight. The average PM we adopted for the cluster is close to those listed by SIMBAD, $\mu_\alpha \cos \delta \approx -35.99 \pm 0.14$ mas yr^{-1}, and $\mu_\delta \approx -12.92 \pm 0.14$ mas yr^{-1} (Loktin & Beshenov 2003). Naturally, around the peak of the cluster, the distribution is dominated by members, and away from the peak the contamination by field stars becomes prominent. In fact, Praesepe is among a few cases where the cluster's motion is clearly separated from that of the
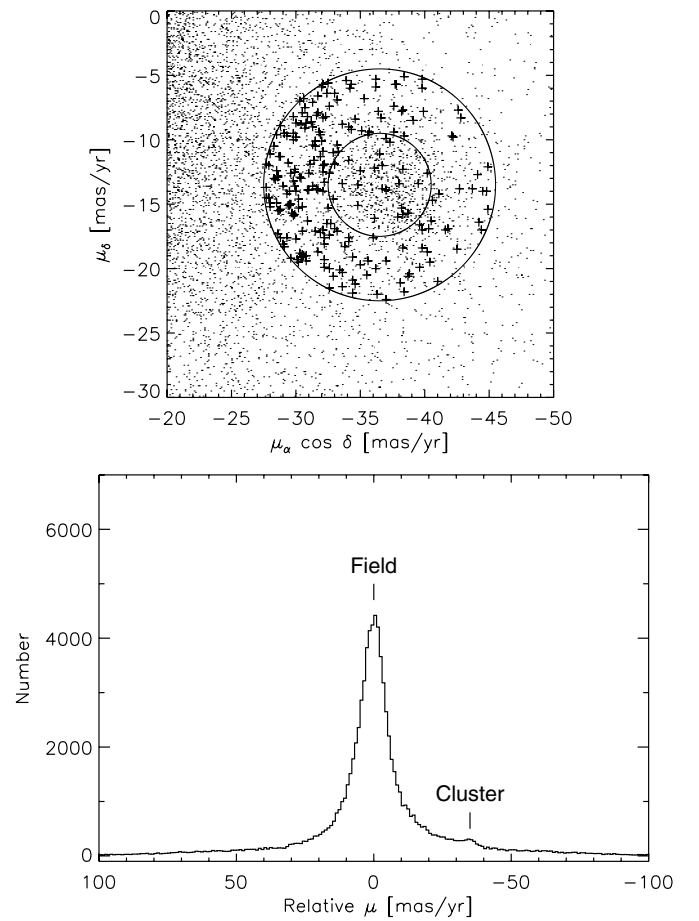

Figure 2. 2MASS/PPMXL stars toward Praesepe. Top: the proper motion distribution. The two circles illustrate the proper motion ranges of $\Delta\mu = 4$ mas yr^{-1} and of $\Delta\mu = 9$ mas yr^{-1}, respectively. Stars within $\Delta\mu = 9$ mas yr^{-1}, but otherwise outside the cluster region (beyond 3°), and photometrically not following the cluster isochrone, i.e., field stars, are marked with crosses. Bottom: the projected PM distribution along the line connecting the field centroid and the cluster centroid. The bump near -35 mas yr^{-1} is due to the cluster, which has a standard deviation of 9 mas yr^{-1} when fitted with a Gaussian function.

field, so the PM distribution exhibits a distinct secondary peak due to the cluster.

We exercised two levels of PM selection. First, a Gaussian function was fitted to the secondary (cluster) peak. Even though the distribution is known to be non-Gaussian (Girard et al. 1989), the top part of the peak can be reasonably approximated by a Gaussian with a standard deviation of 9 mas yr^{-1}. This is the PM range, namely within $\Delta\mu = 9$ mas yr^{-1} of the cluster's average PM, that we adopted to select PM membership. This range is similar to that used by Kraus & Hillenbrand (2007; 8 mas yr^{-1}) or by Boudreault et al. (2012; 8 mas yr^{-1} in $\Delta\mu_\alpha \cos \delta$ and 12 mas yr^{-1} in $\Delta\mu_\delta$). We note that Boudreault et al. (2012) derived a different mean motion, ($\mu_\alpha \cos \delta = -34.17 \pm 2.74$ mas yr^{-1}, $\mu_\delta = -7.36 \pm 4.17$ mas yr^{-1}), using relative PMs on the basis of the UKIDDS data. This discrepancy may arise because, though both authors used the median value to choose the center of the PM range, the distribution is skewed because of the contribution from the field. The next level of PM selection is $\Delta\mu = 4$ mas yr^{-1}, at which there is about the same contribution from the cluster and the field, i.e., a 50% contamination of the sample. Figure 2 compares the cases of 4 versus 9 mas yr^{-1}. While bright candidates, including giant stars, are not greatly affected by the choice, the cluster sequence
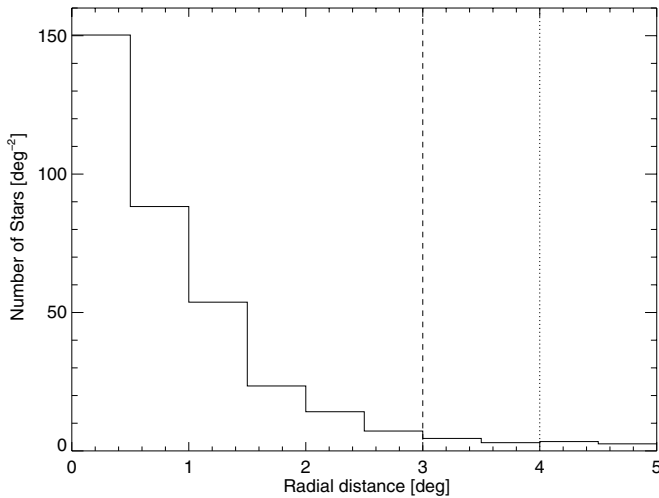
Figure 3. Radial density distribution of all stars within the entire 5° field, satisfying the isochrone and PM criteria. The vertical line at the 3° radius marks the location where we consider the cluster region to be in our analysis. The region between radius 4° (shown by another vertical line) and 5° is used as the field region.

clearly stands out with the narrower PM range, even without restrictions on position, color, or magnitude. The adoption of $\Delta\mu < 9$ mas yr^{-1} facilitates a comparison between our results and previous works. However, the $\Delta\mu < 4$ mas yr^{-1} sample was saved for a more reliable selection of candidates. Figure 2 also shows the PM distribution projected on the line connecting the peak of the field and the peak of the cluster. Even with this projection showing the maximum distinction between the two peaks, the distribution near the cluster is overwhelmed by that of the field.

Figure 3 shows the radial density profile of stars roughly following the cluster's isochrone and PM within the entire 5° field. The surface density decreases monotonically until it reaches about 3°, then levels off. Therefore, our analysis was conducted within a spatial radius of 3°. At 179 pc, this corresponds to a linear dimension of ∼18 pc across. This size is relatively large among the 1657 entries with both angular diameter and distance determinations in the open cluster catalog compiled by Dias et al. (2002),[12] with the majority having diameters of 2–4 pc.

Figure 4 shows the J versus $J - K_s$ and the $g_{\rm P1}$ versus $g_{\rm P1} - y_{\rm P1}$ CMDs when the spatial (within or beyond 3° angular distance from the cluster center) and PM criteria (within 9 or 4 mas yr^{-1}) are applied. Even without a preselection by photometry or color, the cluster sequence is already evident. A subsample was chosen with a restrictive set of parameters, namely with the angular distance within the central 30′, and with $\Delta\mu = 4$ mas yr^{-1}. This subsample is incomplete but it consists of highly secured members, which validates our initial rough selection ranges of magnitude and colors, and it can be used to compare various stellar atmospheric models.

For the 2MASS/PPMXL sample, photometric candidacy is selected in the J versus $J - K_s$ CMD (1) for stars that are brighter than $J \sim 12$ mag, from 0.06 mag below to 0.18 mag above, and perpendicular to the Padova track (for giants there is no photometric restriction, i.e., only the spatial and kinematic criteria were applied) and (2) for fainter stars, from 0.1 mag below to 0.1 mag above, and perpendicular to the Siess isochrone.
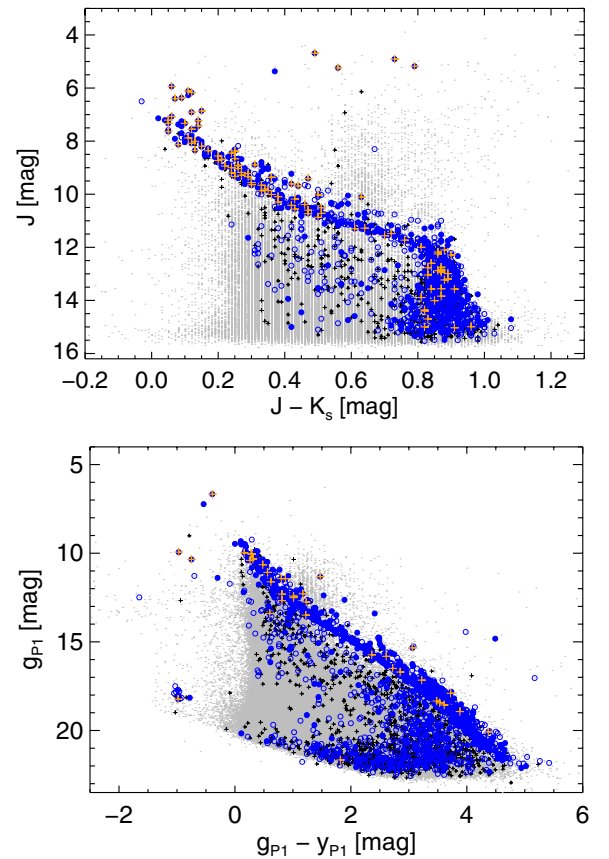
Figure 4. Top: J vs. $J - K_s$ CMD for all the stars (gray dots), those with angular distances greater than 3° from the cluster center but with $\Delta\mu < 9$ mas yr^{-1} (small black crosses), those within 3° from the cluster center and with $\Delta\mu < 9$ mas yr^{-1} (blue open circles), and those within 3° and with $\Delta\mu < 4$ mas yr^{-1} (blue filled circles). The stars at the very center of the cluster, namely within 30′, and with $\Delta\mu < 4$ mas yr^{-1} are highly probable members and are marked as orange crosses. Note the group of blue stragglers beyond the main sequence turn-off point (Andrievsky 1998). Bottom: $g_{\rm P1}$ vs. $g_{\rm P1} - y_{\rm P1}$ CMD, with the same symbols as in the top panel. The group of stars near $g_{\rm P1} = 18$ mag, and $g_{\rm P1} - y_{\rm P1} = -1$ mag include white dwarfs known in the cluster (Dobbie et al. 2004, 2006).

(A color version of this figure is available in the online journal.)

For stars fainter than the 2MASS sensitivity, we resorted to the PS1 data collected through 2012 January. The luminosity function toward Praesepe reaches beyond $g_{\rm P1} \sim 21.5$ mag, but our data are limited by the sensitivity of the PPMXL data set at around 21 mag. To avoid spurious detections, only sources that have been measured more than twice in both $g_{\rm P1}$ and $y_{\rm P1}$ bands were included in our analysis. The $g_{\rm P1}$ magnitudes were derived from the SDSS magnitudes (taken from Kraus & Hillenbrand 2007) and transformed to the PS1 photometric system (Tonry et al. 2012b), namely by $g_{\rm p1} = g_{\rm SDSS} - 0.012 - 0.139\,x$, where $x = (g - r)_{\rm SDSS}$. For the $y_{\rm P1}$ magnitudes, because SDSS has no corresponding y, the transformation from $z_{\rm SDSS}$ was used, $y_{\rm P1} = z_{\rm SDSS} + 0.031 - 0.095\,x$, where x is again $(g - r)_{\rm SDSS}$. Because of this, and due to the Paschen absorption, the transformation to $y_{\rm P1}$ (and to $z_{\rm P1}$) has a larger uncertainty than in other bands (Tonry et al. 2012b). In the transformation to either $g_{\rm P1}$ or $y_{\rm P1}$, using the quadratic instead of the linear fit makes little difference. The bottom panel of Figure 4 plots $g_{\rm P1}$ versus $g_{\rm P1} - y_{\rm P1}$ together with the PS1 main sequence, transformed from Kraus & Hillenbrand (2007). For the PS1/PPMXL sample, the selection range is from 0.15 mag below to 0.4 mag above and perpendicular to the

Kraus & Hillenbrand (2007) main sequence, transformed to the PS1 system (Tonry et al. 2012b).

Together, the 2MASS/PPMXL and the PS1/PPMXL samples contain a total of 1040 stars that satisfy all the criteria of photometry (along the isochrone), kinematics (consistent PMs), and spatial (within a 3° radius) grouping. There are 168 stars satisfying the same set of criteria, but with radii between 4° and 5° (which happens to have the same sky area as the 3° cluster radius, i.e., 9π deg^2)—these are considered field stars, and should be subtracted from the cluster region. So our final list contains 1040 member candidates, among which about 872 (∼84%) should be true cluster members. Statistically, a brighter candidate is more likely to be a true member than a fainter candidate because of the field contamination. If the stringent criterion of $\Delta\mu = 4$ mas yr^{-1} had been used instead, the number of candidates would have become 547 within 3°, and 33 between 4° and 5°, yielding a net of 514 members within 3°, and a 6% false positive rate.

4. THE UPDATED MEMBER LIST

Table 1 lists the properties of the 1040 candidates. The first two columns, 1 and 2, provide identification numbers and coordinates. Columns 3 and 4 provide the PM measurements and errors in right ascension and declination, taken from the PPMXL catalog. Subsequent columns, 5 to 12, list the photometric magnitudes and corresponding errors of PS1 g_{P1}, r_{P1}, i_{P1}, z_{P1}, and y_{P1}, and 2MASS J, H, and K_s. Column 13 indicates whether the candidate could possibly be binary, and the last column, 14, lists the common star names, if any. The 2MASS and PS1 CMDs of the members listed in Table 1 are displayed in Figure 5, along with the selected stellar models: BT-Settl (Allard et al. 2013; Allard 2014),[13] Siess et al. (2000), Padova (Marigo et al. 2008), and Kraus & Hillenbrand (2007). To convert the effective temperature in the Siess et al. (2000) models to J, H, and K_s magnitudes, we made use of the table presented in Kenyon & Hartmann (1995). While all isochrones roughly follow each other for $J \lesssim 12$ mag, they noticeably differ toward faint magnitudes. The Padova isochrone is too blue to fit the data. This cannot be explained by reddening because Praesepe is very nearby and is hardly reddened ($E(B - V) = 0.027$ mag; Taylor 2006). The four other stellar models fit the data quite well, though they diverge toward the lowest mass end of our data. The highly secure list of candidates indicates a better fit with the BT-Settl model.

Our member candidates have been grouped by using five out of six dimensional photometric and kinematic parameters, lacking only the radial velocity measurements. Hence, our list is more reliable than using photometry alone, and is more comprehensive, in terms of stellar mass and sky area coverage than other lists that are currently available. Among the 1040 candidates, 214 were selected from the 2MASS/PPMXL sample, 82 were selected from the PS1/PPMXL sample, and 742 were selected from both. Aside from the limit at the bright end, the reason that PS1/PPMXL does not find more candidates is because the faintest candidates are very red, $g_{P1} - K_s \approx 7$ mag—in favor of 2MASS detection—and because the PS1/PPMXL data are limited by the brightness limit of PPMXL. The situation will improve once PS1 produces its own PM measurements. A total of 890 of our candidates coincide with those of Kraus & Hillenbrand (2007), 567 with those of
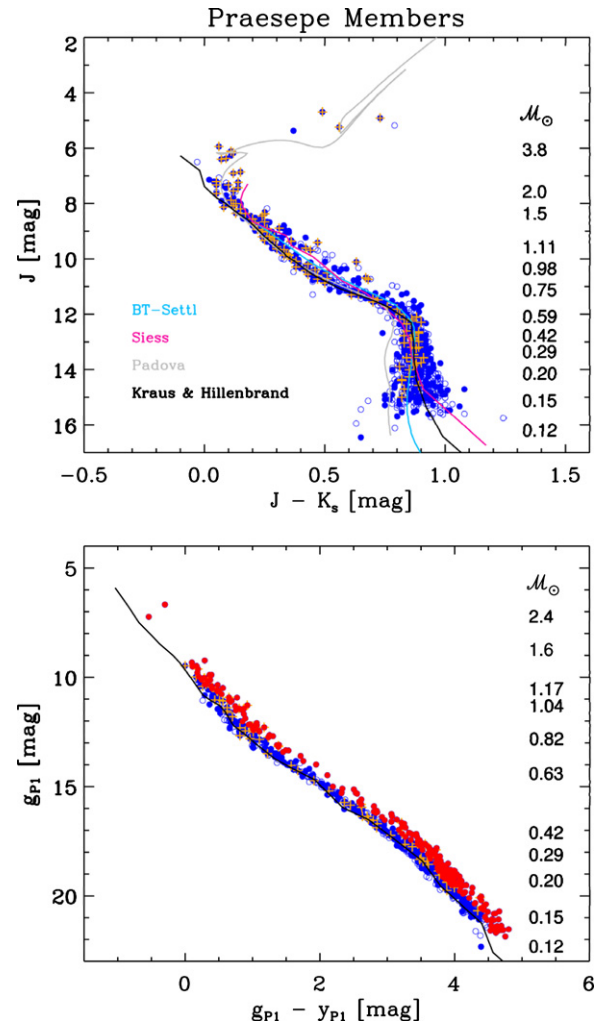

Figure 5. Member candidates in Praesepe selected on the basis of position, proper motion, and magnitude/color. Top: the J vs. $J - K_s$ CMD, together with the stellar models of BT-Settl (Allard et al. 2013; Allard 2014), Siess, Padova, and Kraus & Hillenbrand (2007). Selected stellar mass values are labeled. Symbols are the same as in Figure 4. Bottom: the g_{P1} vs. $g_{P1} - y_{P1}$ CMD for candidates. The solid curve is the main sequence from Kraus & Hillenbrand (2007) transformed to the PS1 system. Red symbols mark possible binaries.
(A color version of this figure is available in the online journal.)

Boudreault et al. (2012), and 190 with neither. Of the latter, 96 candidates have not been identified in either Hambly et al. (1995b), Pinfield et al. (1997), Adams et al. (2002), or Baker et al. (2010). Some of our candidates, missed by Boudreault et al. (2012), are located in the UKIDSS survey gap.

Membership identification by photometry alone, e.g., by González-García et al. (2006) and Boudreault et al. (2010), is vulnerable to significant contamination by field stars, so reliable membership could be secured for bright stars only. To illustrate this, the entire PS1/PPMXL 5° sample contains 320,312 stars. There would have been 2445 candidates if only the photometric and positional criteria were set, but the number reduces drastically to 826 once the additional PM criterion, ($\Delta\mu \leqslant 9$ mas yr^{-1}), is imposed.

Our member list includes the two stars recently reported by Quinn et al. (2012), BD+20 2184 (their Pr 0201 = NGC 2632 KW 418) and 2MASS J08421149+1916373 (their Pr 0211 = NGC 2632 KW 448), to host exoplanets. A few candidates found in previous works did not pass our PM selection. For example, stars J083850.6+192317 and J084108.0+1914901,

6

Table 1
Member Candidates of Praesepe

No.	R.A. Decl. (J2000) (deg)	$\mu_\alpha \cos\delta$ (mas yr^{-1})	μ_δ (mas yr^{-1})	g_{P1} (mag)	r_{P1} (mag)	i_{P1} (mag)	z_{P1} (mag)	y_{P1} (mag)	J (mag)	H (mag)	K_s (mag)	Flag	Remarks
(1)	(2)	(3)	(4)	(5)	(6)	(7)	(8)	(9)	(10)	(11)	(12)	(13)	(14)
413	129.7619871 19.7248670	-34.8 ± 1.1	-13.6 ± 1.1	12.120 ± 0.001	...	...	...	...	8.366 ± 0.026	8.126 ± 0.021	8.125 ± 0.021	0	BD+20 2140
414	129.7620587 19.5325438	-37.5 ± 4.1	-16.9 ± 4.1	17.618 ± 0.005	16.347 ± 0.002	15.095 ± 0.600	14.364 ± 0.001	14.060 ± 0.003	12.829 ± 0.022	12.182 ± 0.021	11.962 ± 0.019	1	
415	129.7627808 19.4043081	-38.9 ± 4.1	-16.2 ± 4.1	19.373 ± 0.018	18.124 ± 0.009	16.549 ± 0.003	15.841 ± 0.002	15.494 ± 0.003	14.261 ± 0.027	13.643 ± 0.027	13.407 ± 0.035	1	
416	129.7633143 20.0437781	-44.3 ± 4.1	-13.7 ± 4.1	14.975 ± 0.001	13.827 ± 0.001	13.489 ± 0.600	13.074 ± 0.001	12.927 ± 0.001	11.867 ± 0.023	11.209 ± 0.021	11.051 ± 0.022	0	
417	129.7651196 19.9997784	-31.5 ± 1.1	-12.6 ± 1.3	...	...	...	12.844 ± 0.002	12.690 ± 0.002	7.860 ± 0.023	7.819 ± 0.016	7.769 ± 0.018	0	HD 73430
418	129.7663424 20.5672773	-38.0 ± 4.1	-11.3 ± 4.1	17.691 ± 0.006	16.496 ± 0.003	15.336 ± 0.600	14.615 ± 0.001	14.342 ± 0.002	13.108 ± 0.025	12.464 ± 0.024	12.276 ± 0.021	1	
419	129.7670607 19.5226714	-37.4 ± 4.1	-12.3 ± 4.1	14.274 ± 0.001	13.482 ± 0.600	13.076 ± 0.600	12.831 ± 0.600	12.601 ± 0.001	11.562 ± 0.022	10.987 ± 0.019	10.857 ± 0.016	0	
420	129.7712342 19.7573463	-36.1 ± 4.1	-15.6 ± 4.1	19.064 ± 0.016	17.807 ± 0.009	16.395 ± 0.600	15.616 ± 0.001	15.289 ± 0.003	14.010 ± 0.024	13.424 ± 0.030	13.164 ± 0.028	1	
421	129.7717692 20.1172023	-35.1 ± 1.1	-14.3 ± 1.2	9.489 ± 0.600	9.354 ± 0.600	9.347 ± 0.600	9.375 ± 0.600	9.383 ± 0.600	8.603 ± 0.030	8.455 ± 0.026	8.413 ± 0.027	0	HD 73429
422	129.7754141 19.6768137	-33.7 ± 1.2	-13.9 ± 1.2	7.539 ± 0.600	7.519 ± 0.600	7.559 ± 0.600	7.573 ± 0.600	7.586 ± 0.600	6.857 ± 0.026	6.769 ± 0.023	6.708 ± 0.018	0	HD 73449

(This table is available in its entirety in a machine-readable form in the online journal. A portion is shown here for guidance regarding its form and content.)

listed by González-García et al. (2006) as members on the basis of optical and infrared photometry, have PMs ($\mu_\alpha \cos \delta = 197.5$ mas yr^{-1} and $\mu_\delta = 79.6$ mas yr^{-1} for J083850.6+192317, and $\mu_\alpha \cos \delta = -58.4$ mas yr^{-1}, and $\mu_\delta = 24.9$ mas yr^{-1} for J084108.0+1914901) that are inconsistent with being part of Praesepe. Another highly probable member suggested by González-García et al. (2006), J084039.3+192840, which has already been refuted by Boudreault et al. (2010) because of its ($I_c - K_s$) color, is not included in our candidate list.

Of the six brown dwarf candidates proposed by Boudreault et al. (2010, their Table 5), only three are found in our data, though the identification of stars No. 099 and No. 909 is uncertain due to the presence of a nearby star in each case (see the finding charts in their Figure 8). Only star No. 910 may have a PPMXL counterpart within $10''$, but it has a PM ($\mu_\alpha \cos \delta = -10.5 \pm 7.3$ mas yr^{-1}, $\mu_\delta = -10.7 \pm 7.3$ mas yr-1) that is inconsistent with membership. The brown dwarf candidate found by Magazzù et al. (1998), NGC 2632 Roque Praesepe 1, was not in our list because of its faint magnitude ($J = 21.0$ mag).

van Leeuwen (2009) identified 24 *Hipparcos* members in Praesepe, but did not tabulate them. With the identifications kindly provided by van Leeuwen, we confirm that they are all enlisted in our candidate sample. The blue stragglers in the cluster suggested by Andrievsky (1998), HD 73666, HD 73819, HD 73618, and HD 73210, are too bright for PS1, and are all confirmed to be PM members. Our photometric selection precludes the white dwarfs known in the cluster (Dobbie et al. 2004, 2006). They are too faint for 2MASS but have been recovered by PPMXL and PS1, illustrated in Figure 4. One additional white dwarf candidate is identified in our data ($\alpha = 127°166145$, $\delta = +19°728674$, J2000; $\mu_\alpha = -40.4 \pm 5.2$ mas yr^{-1}, $\mu_\delta = -20.4 \pm 5.2$ mas yr^{-1}) with $g_{P1} = 18.15$ mag, and $y_{P1} = 19.07$ mag. The white dwarf members follow the general cooling sequence, from brighter/bluer to fainter/redder in the CMD. Scaled with white dwarfs in the field, and studied by Tonry et al. (2012a) who also used PS1 data, the ones in Praesepe have a cooling timescale of 0.2–0.4 Gyr.

4.1. Binary Fraction

In a binary system with identical component stars the brightness of either star would be overestimated by 0.75 mag. Therefore, a binary sequence is often seen as a swath up to 0.7–0.8 mag above the main sequence of a star cluster in a CMD. Multiple systems may have even larger magnitude differences. Steele & Jameson (1995) and Hodgkin et al. (1999) estimated a multiplicity of $\sim$0.5 for low-mass members in Praesepe. In both the 2MASS and PS1 CMDs (see Figure 5), the binary sequence clearly stands out. Such a distinct binary sequence was already noticed by Kraus & Hillenbrand (2007). Note that the J versus $J - K_s$ main sequence is characterized by a slanted upper part and turns nearly vertically below the mass of $\sim$0.6 $M_\odot$. While the upper main sequence allows us to gauge the distance (shifting vertically), the vertical segment provides a convenient tool to estimate the reddening of a cluster (shifting horizontally). This fact, however, also means that the J versus $J - K_s$ CMD cannot be used to evaluate the binarity at the lower main sequence. Instead, the PS1 CMD shows a monotonic track, so it is useful for this purpose.

There is no clear dividing line above the main sequence to separate binaries from single stars. The bottom panel of Figure 5 demonstrates a magnitude difference of 0.5 mag above the main sequence as the dividing line. In this case, there are 242 stars above the line, or a binary fraction of about 23% of the total 1040 member candidates. No attempt was made to separately estimate the binarity of the 872 true member versus the 168 interloper samples. If the difference is lowered to 0.4 mag or 0.3 mag, the number increases to 302 (29%) or 389 (37%), respectively. The relatively small increase in the binary fraction is the consequence of a distinct binary sequence of this cluster; that is, the binaries in Praesepe tends to be of similar-mass systems, as noted, for example, by Pinfield et al. (2003). It also seems to teem with multiple systems, as concluded by Khalaj & Baumgardt (2013). Boudreault et al. (2012) conducted an elaborative analysis on the binarity. Adopting a brightness range from 0.376 to 1.5 mag above the (single star) main sequence, these authors derived a binary frequency of 23.3% $\pm$ 7.3% for the mass range of 0.45–0.2 $M_\odot$, 19.6% $\pm$ 3.8% for 0.2–0.1 $M_\odot$, and 25.8% $\pm$ 3.7% for 0.1–0.07 $M_\odot$. Given the uncertainties in membership and binarity assignments, our data do not justify the division of the sample into different mass bins, and we infer an overall binary frequency (or multiplicity) of at least 20%–40%.

4.2. Cluster Mass Function

The stellar mass was interpolated via a least-square polynomial fitting to the J (if too bright in PS1) or g_{P1} magnitude using the compilation of Kraus & Hillenbrand (2007) (their Table 5), and adopting a distance modulus of 6.26 mag. The g_{P1} band observations saturate around $g_{P1} \sim 14$ mag, corresponding to $J \sim 11.5$ mag in our sample, or about 0.6 $M_\odot$. The masses of our candidates range from $\sim$0.11 $M_\odot$ to $\sim$2.39 $M_\odot$.

The luminosity function of the cluster was derived from the subtraction of the field contamination. For field stars, we selected the stars satisfying the same PM and isochrone criteria, but with angular distances between $4°$ and $5°$ from the cluster center. In Figure 6, the g_{P1} luminosity function of the member candidates listed in Table 1 is subtracted by that of the field. The field distribution is flat, as expected, and contributes only a small correction to the observed luminosity function. The corrected luminosity function rises spuriously near the PS1 saturation limit of $g_{P1} \sim 11$–15 mag, and then turns around near $g_{P1} \sim 18$ mag, or mass $\sim$0.3 $M_\odot$.

The mass function of Praesepe members is shown in Figure 7. We note that this is the mass function of the stellar systems, i.e., with no binary correction. Using the optical I_c band and near-infrared J and K_s photometric data, Boudreault et al. (2010) reported a rising mass function, ranging from 0.6 $M_\odot$ to 0.1 $M_\odot$, then turning over. These results are in agreement with previous works, e.g., by Hambly et al. (1995b). This increase in number with decreasing mass was shown by Wang et al. (2011) to continue into the brown dwarf regime, peaking around 70 $M_{\rm Jup}$ then decreasing until about 50 $M_{\rm Jup}$. Kraus & Hillenbrand (2007) and Baker et al. (2010) also derived a rising, but flatter, mass function. On the other hand, Boudreault et al. (2012), also using the UKIDSS photometry but adding additional PM information, obtained a contradictory result, namely, a declining mass function between 0.6 $M_\odot$ and 0.1 $M_\odot$, which is different from that obtained by Hambly et al. (1995b), Chabrier (2005), Kraus & Hillenbrand (2007), Baker et al. (2010), and Boudreault et al. (2010). Our sample is more complete than that of Boudreault et al. (2012) at the higher mass end, but the mass function is otherwise consistent with theirs in regards to having stellar masses greater than around 0.3 $M_\odot$. Overall, the mass function we obtained resembles that of the disk population (Chabrier 2005) for the massive part, but shows a deficit in the lowest mass population ($\lesssim$0.3 $M_\odot$).
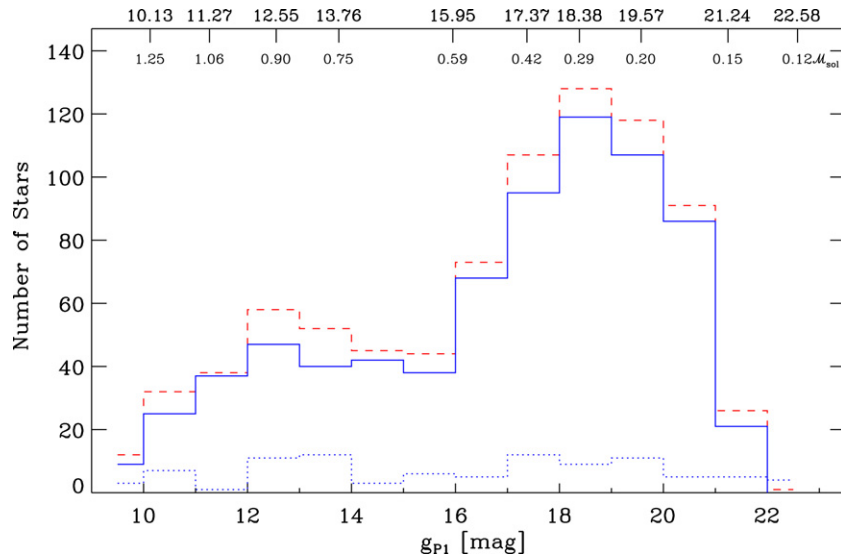
Figure 6. Observed g_{P1} luminosity function of member candidates (the red dashed line) is subtracted by the field population with the same photometric and PM selection criteria (blue dotted line) to derive the corrected cluster luminosity function (solid blue line). The corresponding stellar mass is labeled at the top in units of solar mass.

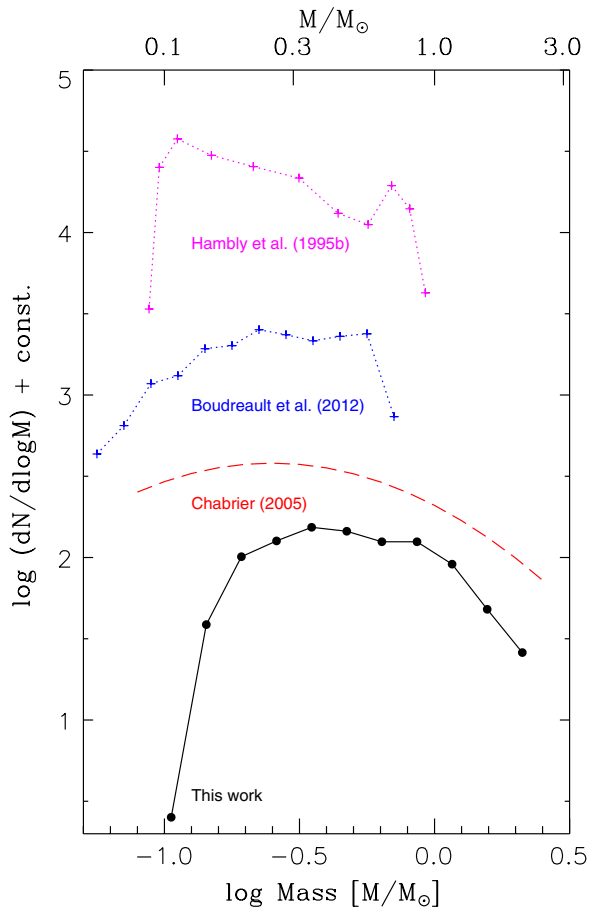(A color version of this figure is available in the online journal.)

Figure 7. Mass function of Praesepe (solid line). The mass function of the disk population by Chabrier (2005; long-dashed line) and the mass function of Praesepe as found by Hambly et al. (1995b; representing a rising mass function) and Boudreault et al. (2012; representing a falling mass function) (representing a falling mass function; dashed lines) are also shown. Each is shifted vertically for clarity.

(A color version of this figure is available in the online journal.)

4.3. Spatial Distribution of Members

Even the youngest star clusters may have an elongated shape (Chen et al. 2004), which is likely a consequence of a filamentary structure in the parental clouds. Subsequent encounters among member stars then circularize the core of a cluster. Mass segregation occurs as energy losing massive stars sink to the center, whereas lower-mass members gain energies and occupy a larger volume in space. Some stars may gain speed sufficient enough to escape the system. The lowest mass members are particularly vulnerable to such stellar "evaporation." As the cluster evolves, the internal gravitational pull becomes weaker and external disturbances, such as differential rotation or tidal force from passing molecular clouds and the Galactic disk, act together to distort the shape of a cluster and eventually tear it apart. Deformation and tidal stripping are even effective for globular clusters (Chen & Chen 2010).

Figure 8 shows how the stellar mass correlates with the spatial distribution. The radial density profiles have been computed for four different mass groups: $M/M_\odot \leqslant 0.2$ (129 stars), $M/M_\odot = 0.2$–0.35 (256 stars), $M/M_\odot = 0.35$–0.7 (332 stars), and $M/M_\odot \geqslant 0.7$ (323 stars). The top panel shows the observed density profiles, while the bottom panel compares the normalized profiles. Because of the normalization, no correction of the field contamination is necessary. Relatively massive members appear to be centrally concentrated, whereas lower mass members are more scattered spatially, a result of mass segregation.

Mass segregation in Praesepe was well demonstrated by Hambly et al. (1995b), Kraus & Hillenbrand (2007), and Khalaj & Baumgardt (2013). Our result is consistent with that of Hambly et al. (1995b) from 0.85 $M_\odot$ to 0.15 $M_\odot$. When the radial density distribution shown in Figure 8 is parameterized with an exponential form, $\sigma(r) \propto e^{-\alpha r}$, the least-squares fitting yields $\alpha = 2.21$ (for members >0.7 $M_\odot$), 0.96 (0.35–0.7 $M_\odot$), and 0.42 (0.2–0.35 $M_\odot$). Caballero (2008) suggested that a power-law function may be more appropriate. In any case, for the faintest sample, the density distribution is certainly not exponential. Instead, it exhibits a sharp truncation beyond 1°.
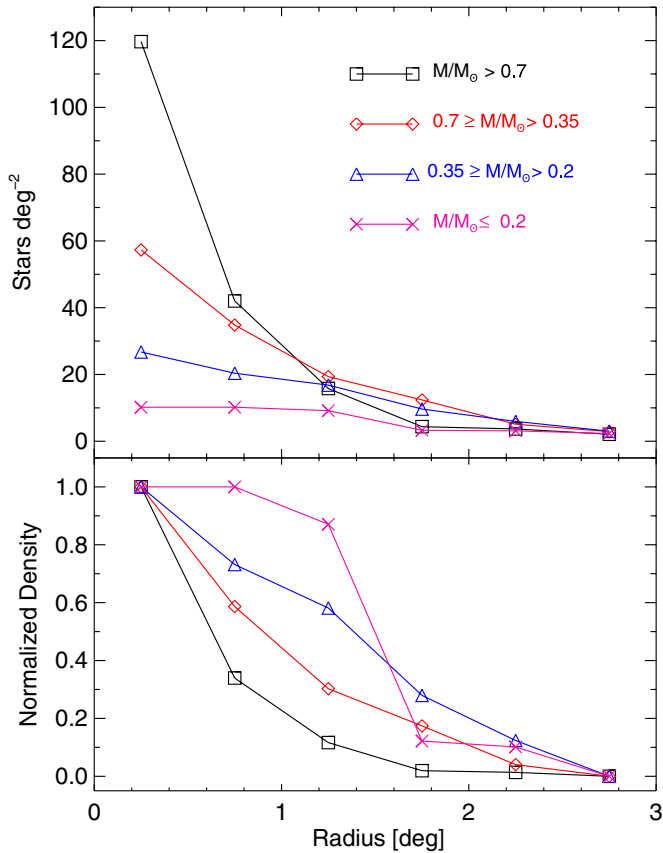
Figure 8. Radial density distribution of the members. The lines with different colors show different magnitude ranges. The top panel shows each derived distribution and the bottom panel shows the same, but normalized from unity at the center to zero at the edge of the cluster.

(A color version of this figure is available in the online journal.)

Figure 9. Positional distributions of stars more massive (open circles) and less massive (solid circles) than 0.35 $M_\odot$.

(A color version of this figure is available in the online journal.)

Figure 10. Proper motion distributions for the same two mass groups of members as shown in Figure 9.

(A color version of this figure is available in the online journal.)

We interpret this as a consequence of stellar evaporation, which further supports the notion of a relative lack of low-mass stars in Praesepe, as already demonstrated in Figure 7.

Mass segregation is further manifested by the positional (Figure 9) and PM distributions (Figure 10) of the members; namely, relatively massive members are concentrated in a smaller volume in space, and have a smaller velocity dispersion than lower-mass stars. The average stellar mass in our sample is $\bar{m} \approx 0.59\,M_\odot$, close to that of a Miller–Scalo initial mass function. With the total number of members equaling $N = 872$, the total stellar mass in the cluster amounts to at least $\sim 520\,M_\odot$. The lowest mass stars, with a declining mass function, do not contribute significantly to the total mass. With a radius of $R = 9$ pc, the velocity dispersion of the cluster would be $v \approx (GN\bar{m}/R)^{1/2} = 0.5$ km s^{-1}, which is noticeably less than the typical value of 1–2 km s^{-1} for Galactic open clusters. At the assumed distance of 179 pc to Praesepe, an intracluster PM dispersion of 1 mas yr^{-1} corresponds to a velocity dispersion of 0.8 km s^{-1}. Thus, our data are not precise enough to measure the PM gradient among members.

There is mounting evidence suggesting that Praesepe is dissolving. It is spatially extended with a sparse stellar density. Holland et al. (2000) suggested that Praesepe might consist of two merging clusters. The relatively high fraction of equal mass pairs (and of multiples) may be the consequence of occasional stellar ejection during three-body encounters (Binney & Tremaine 1987), or during the merging process. Relevant timescales for a dissolving star cluster include (1) the dynamical
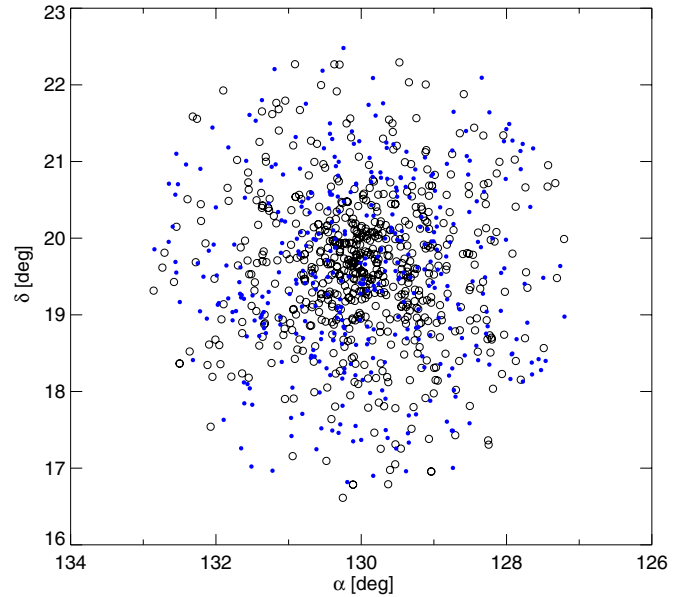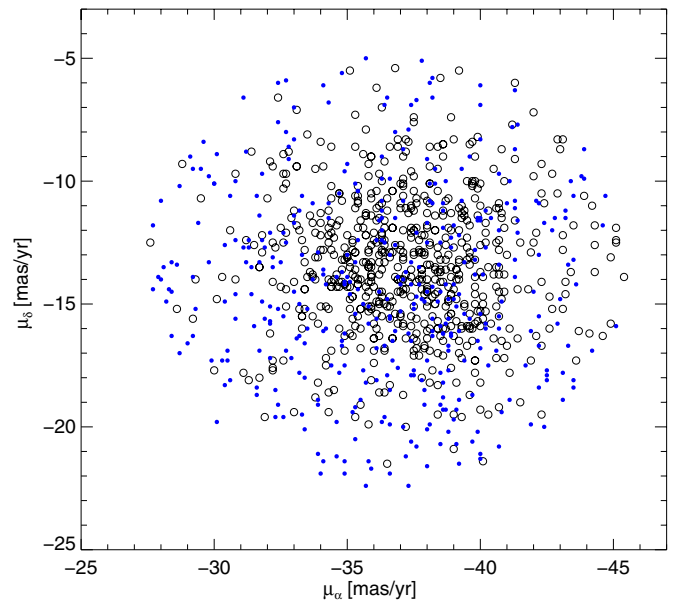
(crossing) timescale, $\tau_{\rm dyn} \approx 2R/v$, (2) the relaxation time, $\tau_{\rm relax} \approx \tau_{\rm dyn}\,0.1\,N/\ln N$, and (3) the evaporation time, $\tau_{\rm evap} \approx 100\,\tau_{\rm relax}$ (Binney & Tremaine 1987). For Praesepe, these timescales are $\tau_{\rm dyn} = 3.6 \times 10^7$ yr, $\tau_{\rm relax} = 4.6 \times 10^8$ yr, and $\tau_{\rm evap} = 4.6 \times 10^{10}$ yr, respectively. The lowest-mass members, having an average escape probability (Spitzer 1987) several times of that for the most massive stars, are particularly susceptible to ejection. The Praesepe cluster therefore is almost fully relaxed, and tidal stripping has occurred, starting with the lowest mass members which have been observed escaping from the cluster.

5. SUMMARY

We have conducted a photometric and PM selection of the member stars of the Galactic open cluster Praesepe, using 2MASS, PPMXL, and Pan-STARRS data. Our sample is comprehensive in terms of sky area ($3°$ radius), limiting magnitude ($g_{P1} \sim 21$ mag), and reliability ($\sim 16\%$ false positive rate). A total of 1040 member candidates are identified, 872 of which are highly probable members, down to about 0.1 solar masses. While for members more massive than $0.6\,M_\odot$, the Padova isochrone works well, the BT-Settl atmospheric model fits better toward fainter magnitudes. The binary frequency of Praesepe members is about 20%–40%, with a relatively high occurrence of similar mass pairs. The mass function is consistent with that of the disk population, but with a deficit of stars less massive than $0.3\,M_\odot$. Members show a clear evidence of mass segregation, with the lowest mass population being evaporated from the system. At the faint magnitude end, the sensitivity of the PM measurements remains the bottleneck of membership selection for very faint objects. Once the PS1 completes its survey in early 2014, increasing the photometric depth and the stellar PM baseline to more than 3.5 yr, we expect to secure member lists for nearby star clusters well into the substellar regime.

REFERENCES

Abazajian, K. N., Adelman-McCarthy, J. K., Agüeros, M. A., et al. 2009, ApJS, 182, 543
Adams, J. D., Stauffer, J. R., Skrutskie, M. F., et al. 2002, AJ, 124, 1570
Allard, F. 2014, in IAU Symp. 299, Exploring the Formation and Evolution of Planetary Systems, ed. M. Booth, B. C. Matthew, & J. R. Graham (Cambridge: Cambridge Univ. Press), 271
Allard, F., Homeier, D., & Freytag, B. 2013, MmSAI, 84, 1053
An, D., Terndrup, D. M., Pinsonneault, M. H., et al. 2007, ApJ, 655, 233
Andrievsky, S. M. 1998, A&A, 334, 139
Asplund, M., Grevesse, N., Sauval, A. J., & Scott, P. 2009, ARA&A, 47, 481
Baker, D. E. A., Jameson, R. F., Casewell, S. L., et al. 2010, MNRAS, 408, 2457
Binney, J., & Tremaine, S. 1987, Galactic Dynamics (Princeton, NJ: Princeton Univ. Press)
Boudreault, S., Bailer-Jones, C. A. L., Goldman, B., Henning, T., & Caballero, J. A. 2010, A&A, 510, A27

Boudreault, S., & Lodieu, N. 2013, MNRAS, 434, 142
Boudreault, S., Lodieu, N., Deacon, N. R., & Hambly, N. C. 2012, MNRAS, 426, 3419
Bouvier, J., Kendall, T., Meeus, G., et al. 2008, A&A, 481, 661
Caballero, J. A. 2008, MNRAS, 383, 375
Carrera, R., & Pancino, E. 2011, A&A, 535, A30
Chabrier, G. 2005, in The Initial Mass Function 50 Years Later, ed. E. Corbelli & F. Palle (Astrophysics and Space Science Library, Vol. 327; Dordrecht: Springer), 41
Chappelle, R. J., Pinfield, D. J., Steele, I. A., Dobbie, P. D., & Magazzù, A. 2005, MNRAS, 361, 1323
Chen, C. W., & Chen, W. P. 2010, ApJ, 721, 1790
Chen, W. P., Chen, C. W., & Shu, C. G. 2004, AJ, 128, 2306
de la Fuente Marcos, R., & de la Fuente Marcos, C. 2000, Ap&SS, 271, 127
Dias, W. S., Alessi, B. S., Moitinho, A., & Lépine, J. R. D. 2002, A&A, 389, 871
Dobbie, P. D., Napiwotzki, R., Burleigh, M. R., et al. 2006, MNRAS, 369, 383
Dobbie, P. D., Pinfield, D. J., Napiwotzki, R., et al. 2004, MNRAS, 355, L39
Eggen, O. J. 1960, MNRAS, 120, 540
Gáspár, A., Rieke, G. H., Su, K. Y. L., et al. 2009, ApJ, 697, 1578
Girard, T. M., Grundy, W. M., López, C. E., & van Altena, W. F. 1989, AJ, 98, 227
Goldman, B., Röser, S., Schilbach, E., et al. 2012, A&A, 559, A43
González-García, B. M., Zapatero Osorio, M. R., Béjar, V. J. S., et al. 2006, A&A, 460, 799
Hambly, N. C., Steele, I. A., Hawkins, M. R. S., & Jameson, R. F. 1995a, A&AS, 109, 29
Hambly, N. C., Steele, I. A., Hawkins, M. R. S., & Jameson, R. F. 1995b, MNRAS, 273, 505
Hauschildt, P. H., Allard, F., & Baron, E. 1999, ApJ, 512, 377
Hodapp, K.W., Siegmund, W. A., Kaiser, N., et al. 2004, Proc. SPIE, 5489, 667
Hodgkin, S. T., Pinfield, D. J., Jameson, R. F., et al. 1999, MNRAS, 310, 87
Høg, E., Fabricius, C., Makarov, V. V., et al. 2000, A&A, 355, L27
Holland, K., Jameson, R. F., Hodgkin, S., Davies, M. B., & Pinfield, D. 2000, MNRAS, 319, 956
Jones, B. F., & Cudworth, K. 1983, AJ, 88, 215
Jones, B. F., & Stauffer, J. R. 1991, AJ, 102, 1080
Kaiser, N., Burgett, W., Chambers, K., et al. 2010, Proc. SPIE, 7733, 77330E
Khalaj, P., & Baumgardt, H. 2013, MNRAS, 434, 3236
Klein Wassink, W. J. 1927, PGro, 41, 1
Kenyon, S. J., & Hartmann, L. 1995, ApJS, 101, 117
Kraus, A. L., & Hillenbrand, L. A. 2007, AJ, 134, 2340
Loktin, A. V., & Beshenov, G. V. 2003, ARep, 47, 6
Magazù, A., Rebolo, R., Zapatero Osorio, M. R., Martín, E. L., & Hodgkin, S. T. 1998, ApJL, 497, L47
Magnier, E. A., Schlafly, E., Finkbeiner, D., et al. 2013, ApJS, 205, 20
Marigo, P., Girardi, L., Bressan, A., et al. 2008, A&A, 482, 883
Mermilliod, J.-C., Weis, E. W., Duquennoy, A., & Mayor, M. 1990, A&A, 235, 114
Pinfield, D. J., Dobbie, P. D., Jameson, R. F., et al. 2003, MNRAS, 342, 1241
Pinfield, D. J., Hodgkin, S. T., Jameson, R. F., Cossburn, M. R., & von Hippel, T. 1997, MNRAS, 287, 180
Quinn, S. N., White, R. J., Latham, D. W., et al. 2012, ApJL, 756, L33
Reglero, V., & Fabregat, J. 1991, A&AS, 90, 25
Roeser, S., Demleitner, M., & Schilbach, E. 2010, AJ, 139, 2440
Siess, L., Dufour, E., & Forestini, M. 2000, A&A, 358, 593
Skrutskie, M. F., Cutri, R. M., Stiening, R., et al. 2006, AJ, 131, 1163
Spitzer, L. 1987, Dynamical Evolution of Globular Clusters (Princeton, NJ: Princeton Univ. Press)
Spitzer, L., Jr., & Shull, J. M. 1975, ApJ, 201, 773
Steele, I. A., & Jameson, R. F. 1995, MNRAS, 272, 630
Taylor, B. J. 2006, AJ, 132, 2453
Tonry, J. L., Burke, B. E., Isani, S., Onaka, P. M., & Cooper, M. J. 2008, Proc. SPIE, 7021, 702105
Tonry, J. L., Stubbs, C. W., Kilic, M., et al. 2012a, ApJ, 745, 42
Tonry, J. L., Stubbs, C. W., Lykke, K. R., et al. 2012b, ApJ, 750, 99
van Leeuwen, F. 2009, A&A, 497, 209
Wang, J. J., Chen, L., Zhao, J. H., & Jiang, P. F. 1995, A&AS, 113, 419
Wang, W., Boudreault, S., Goldman, B., et al. 2011, A&A, 531, A164
Williams, D. M., Rieke, G. H., & Stauffer, J. R. 1995, ApJ, 445, 359